JOURNAL OF MATERIALS SCIENCE 11 (1976) 913–924

The structure of the unidirectionally solidified Al-Al_2Au eutectic

G. PIATTI, G. PELLEGRINI
Materials Division, J.N.R.C., Euratom, Ispra, Italy

The structure of a number of unidirectionally solidified Al–Al_2Au alloys of eutectic and off-eutectic compositions has been investigated over a wide range of growth rates (1.6×10^{-4} to 1.66×10^{-2} cm sec^{-1}) using a thermal gradient of approximately 80 to 100° C cm^{-1}. The system exhibits an asymmetric coupled growth zone, which widens at high thermal gradient–growth rate ratios. At high solidification rates a broken lamellar structure is obtained, while at low rates a mixed structure with broken lamellae and rods is present. The crystallographic orientation of the phases as determined on different eutectic grains is as follows:

lamellar interface	$\parallel(0\,0\,1)_{Al_2Au} \parallel (0\,1\,1)_{Al}$
	$[1\,1\,0]_{Al_2Au} \parallel [1\,0\,0]_{Al}$
growth direction of lamellae and rods	$\parallel[1\,1\,0]_{Al_2Au} \parallel [1\,0\,0]_{Al}$

while the preferred growth direction for the Al dendrites as well as for the Al_2Au dendrites has been found to be the [1 0 0] direction. The interlamellar spacing varies according to the well known relationship

$$\lambda = A \cdot R^{-n}$$

where R is the growth rate, with $n \simeq 0.37$ for the free-dendrites eutectic structures and $n \simeq 0.49$ for the inter-dendrite eutectic structures.

1. Introduction

A large variety of metallic systems prepared by controlled heat extraction have been studied in recent years in various laboratories. Extensive work has been done particularly in the field of eutectics obtained by unidirectional solidification. This specific field has been reviewed in detail by various authors [1–5].

A point of general interest emerging from the literature is the extent of the eutectic range, towards the off-eutectic compositions, which has been shown to be both growth rate and thermal gradient dependent. At low gradients the extent of the eutectic range increases with increasing growth rate, as found earlier by Tammann and Botschwar [6] and Kofler [7] who introduced the coupled growth concept; and later by Hunt and Jackson [8] and by Cline and Livingston [9]. At high gradients the extent of the eutectic range is proportional to the ratio between the thermal gradient in the liquid ahead of the liquid–solid interface and the growth rate, as shown by Mollard and Flemings [10] on the basis of constitutional supercooling arguments and by Jordan and Hunt [11]. High thermal gradient dependency has also been treated theoretically with perturbation analysis by Cline [12] and Hurle and Jakerman [13]. A more recent work by Burden and Hunt [14] explained, in terms of a competitive growth model, both high and low temperature gradient dependencies, by starting from Jackson's modification [15] of the Tammann–Borschwar–Kofler coupled-zone theory [6–7]. Finally, the kinetics factor, which is important in metal–metalloid systems, has been included by Steen and Hellawell [16] and by Fisher and Kurz [17] in the theoretical description of the problem.

The present work deals with the extent of

the eutectic range by an experimental investigation of the structure (morphology, lamellar spacings, crystallographic features) of several Al–Al_2Au alloys of hypoeutectic, eutectic and hypereutectic compositions directionally solidified using a wide range of growth rates and at high thermal gradients. The eutectic Al–Al_2Au was chosen because some preliminary results [18] showed that a large range of Al–Al_2Au off-eutectic compositions can be solidified with a eutectic-like structure. The most interesting data characterizing the Al–Al_2Au system are summarized as proposed by Hansen and Anderko [19] in Table I.

TABLE I Characteristics of the Al–Al_2Au eutectic [19]

Solute element	Au
Composition	5.0 wt%
	0.7 at.%
Phases	
Matrix	Al-rich solid solution (maximum solubility 0.3 wt% Au)
Second phase	Al_2Au
Eutectic melting point	642° C
Second phase	
Crystal structure	f c c, CaF_2 type
Micro-hardness (Vickers)	219 kg mm^{-2} (measured by authors on bulk specimen)
Melting point	1060° C
Vol % at eutectic temperature	1.99

2. Experimental

A series of thirty alloys containing between 4 and 16 wt% Au has been prepared starting from high purity components, respectively: 99.98 Al and 99.98 Au, by induction furnace melting of the constituents in an Al_2O_3 crucible under a positive pressure or argon. The ingots were first examined microscopically for uniformity and then extruded at 500° C into rods of 10 mm nominal diameter and reduced by cold swaging to 9.5 mm final diameter. The alloy, in rod form, was subsequently unidirectionally solidified in a cylindrical alumina crucible by remelting the extruded rod and withdrawing the crucible from the furnace through a stationary water-spray heat sink. The equipment has been described in detail elsewhere [20]. The solidification rate (R) was varied between 1.6×10^{-4} and 1.66×10^{-2} cm sec^{-1} with a thermal gradient (G) of 80 to 100° C cm^{-1} in the melt.

As the Al–Al_2Au system provides favourable conditions for segregation phenomena at the eutectic temperature, due to the appreciable difference in density (calculated value: 4.20 g cm^{-3}) between the two phases (i.e. the heavier, solid and the liquid phases), the composition of every alloy investigated was determined by chemical analysis of a large sample, 15 cm long, taken from the ingots about half way along their length. In some cases specimens were also taken from the top and the bottom of the ingots in order to observe eventual segregation phenomena along the growth direction.

Metallographic specimens were taken from a fixed location half-way along the ingots and, in some cases, from other locations too. The specimens were examined microscopically after mechanical polishing and electrolytic etching in a water solution of 35 vol% HNO_3 for a period of about 2 sec. In order to examine the eutectic structure three-dimensionally, some specimens were deeply

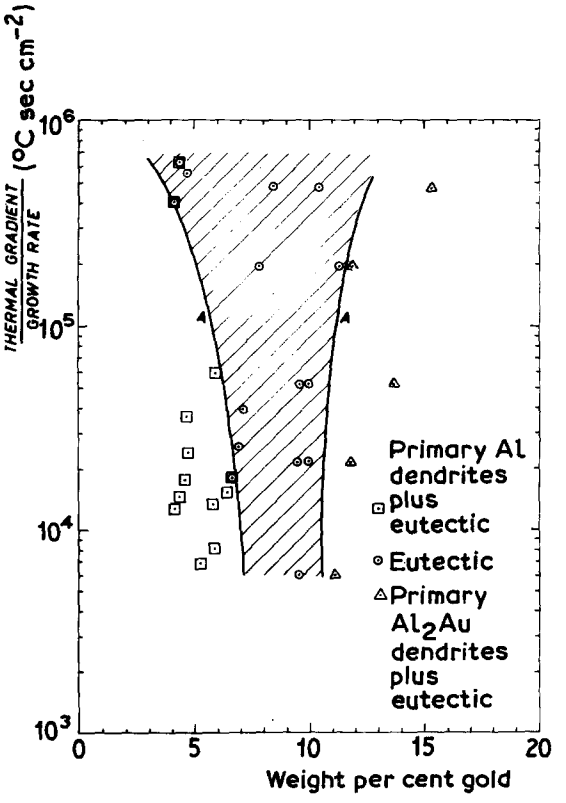

Figure 1 Thermal gradient-growth rate ratio versus alloy composition showing the range of the coupled zone determined for the Al–Al_2Au eutectic system using a thermal gradient of approximately 100° C cm^{-1}. Solid lines show the experimental boundary between dendritic and plane front structures.

etched by removing the Al matrix using the above solution and then observed in a scanning electron microscope. Phase identification and orientation studies were performed using X-rays on various specimens using the techniques described in more detail in Section 3. The dependence of interphase spacing (λ) on the growth rate (R) was determined for alloys of eutectic and hypoeutectic structures. Measurements were made on transverse sections of lamellar-like morphologies using either a microscope ground-glass screen or a photomicrograph. Between 10 and 20 readings were taken for each section and the average value of λ was assigned to the growth rate. A single reading represented the average intercept distance obtained by the line-intercept method for a large number of lamellae. No measurements were taken of the rod-like morphologies.

Finally, some microhardness tests were made on a bulk specimen of intermetallic Al_2Au by means of a Leitz apparatus using 15 g loads (Vickers indentations). The mean value is given in Table I.

3. Results

3.1. Morphology

The principal results revealed by the metallographic observations of the solidified ingots are summarized in Table II, together with the corresponding weight compositions determined by chemical analysis and the corresponding solidification rates and calculated G/R ratios (the value of G was assumed to be $100^\circ C\,cm^{-1}$). The thermal gradient/growth rate ratio versus percentage gold composition is plotted in Fig. 1. From Table II and Fig. 1, it can be observed that (a) the system

TABLE II List of samples

Alloy No.	Composition Type	wt % Au	Growth rate R (cm sec^{-1})	Thermal gradient growth rate G/R ($^\circ$C sec cm^{-2})	Structure
1	Hypoeutectic	4.10	2.5×10^{-4}	4.0×10^5	Some areas primary Al dendrites + eutectic, some areas eutectic
2		4.12	7.9×10^{-3}	1.27×10^4	Primary Al dendrites + eutectic
3		4.36	7.1×10^{-3}	1.41×10^4	Primary Al dendrites + eutectic
4		4.40	1.6×10^{-4}	6.33×10^5	Some areas primary Al dendrites (Fig. 2) + eutectic, some areas eutectic (Figs. 3 and 4)
5	Slightly	4.60	5.8×10^{-3}	1.73×10^4	Primary Al dendrites + eutectic
6	hypoeutectic	4.67	2.77×10^{-3}	3.61×10^4	Primary Al dendrites + eutectic
7		4.71	4.3×10^{-3}	2.32×10^4	Primary Al dendrites + eutectic (Fig. 5)
8		4.71	1.8×10^{-4}	5.55×10^5	Eutectic
9	Slightly	5.23	1.47×10^{-2}	6.80×10^3	Primary Al dendrites + eutectic
10	hypoeutectic	5.80	7.5×10^{-3}	1.33×10^4	Primary Al dendrites + eutectic
11		5.80	1.25×10^{-2}	8.0×10^3	Primary Al dendrites + eutectic
12		5.88	1.66×10^{-3}	6.0×10^4	Primary Al dendrites + eutectic
13	Hypereutectic	6.46	6.66×10^{-3}	1.50×10^4	Primary Al dendrites + eutectic
14		6.68	5.55×10^{-3}	1.80×10^4	Some areas primary Al dendrites + eutectic, some areas eutectic
15		6.92	3.9×10^{-3}	2.56×10^4	Eutectic
16		7.15	2.55×10^{-3}	3.92×10^4	Eutectic (Fig. 6)
17		7.78	5.1×10^{-4}	1.96×10^5	Eutectic
18		8.44	2.1×10^{-4}	4.76×10^5	Eutectic
19		9.44	4.7×10^{-3}	2.13×10^4	Eutectic
20		9.48	1.66×10^{-2}	6.0×10^3	Eutectic
21		9.67	1.91×10^{-3}	5.23×10^4	Eutectic
22		9.83	4.7×10^{-3}	2.13×10^4	Eutectic
23		9.94	1.91×10^{-3}	5.23×10^4	Eutectic
24		10.46	2.1×10^{-4}	4.76×10^5	Eutectic
25		11.13	1.66×10^{-2}	6.0×10^3	Primary Al_2Au dendrites + eutectic
26		11.33	5.1×10^{-4}	1.96×10^5	Eutectic
27	Strongly	11.83	4.7×10^{-3}	2.13×10^4	Primary Al_2Au dendrites + eutectic
28	hypereutectic	11.88	5.1×10^{-4}	1.96×10^5	Primary Al_2Au dendrites + eutectic
29		13.65	1.91×10^{-3}	5.23×10^4	Primary Al_2Au dendrites + eutectic
30		15.35	2.1×10^{-4}	4.76×10^5	Primary Al_2Au dendrites + eutectic (Fig. 7)

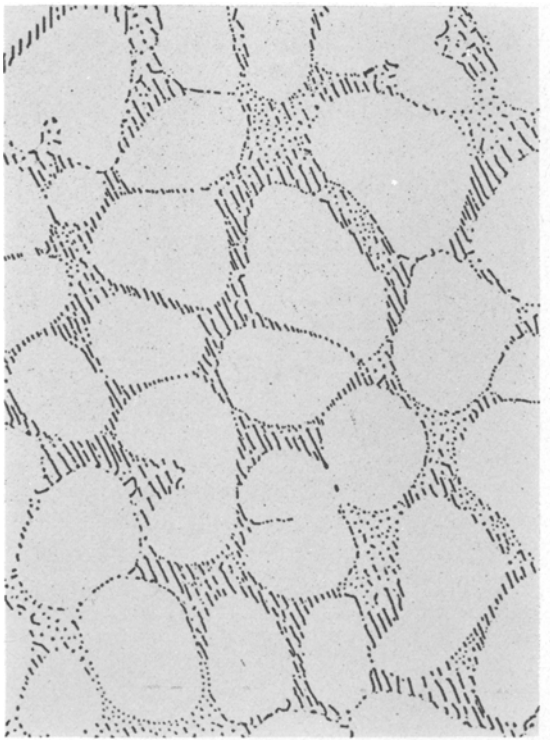

Figure 2 Hypoeutectic structure (optical migrograph) in transverse section of Al–4.40 wt % Au specimen unidirectionally solidified at 1.6×10^{-4} cm sec^{-1} (× 100).

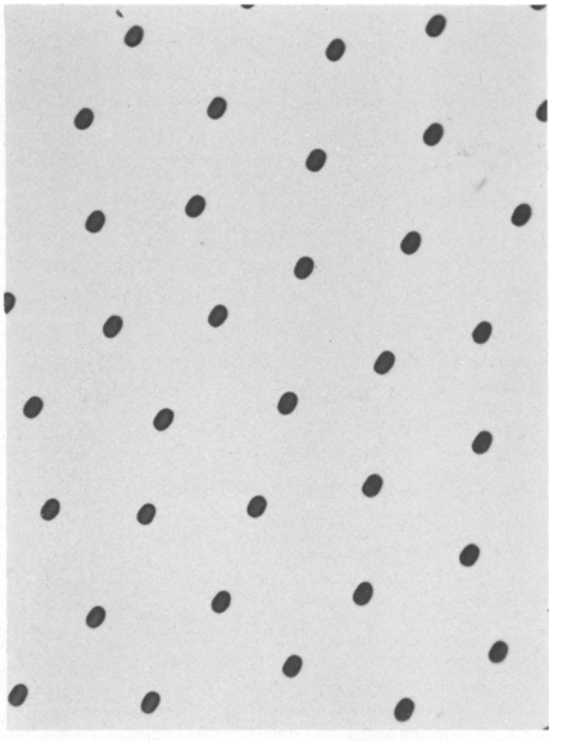

Figure 3 Al_2Au rods (optical micrograph) in transverse section of Al–4.40 wt % Au specimen unidirectionally solidified at 1.6×10^{-4} cm sec^{-1} (× 1000).

exhibits a coupled growth zone skewed toward the hypereutectic compositions, (b) the coupled zone widens at low rates and high gradients, i.e. at high G/R ratios.

The Al–Al_2Au system is also characterized by a broken lamellar morphology (Figs. 2, 4 and 6) which is present at all solidification rates. At low velocities the lamellae appear to be less broken, whilst at high velocities they are finer and more discontinuous. Grains of ordered (Fig. 3), or randomly arranged rods are present; at low velocities their density increases at lower rates and does not seem to depend on solute concentration. Scanning electron microscopy of the rods indicates that they are faceted. This faceted nature of the Al_2Au intermetallic is seen more clearly from the morphology in hypereutectic structures of Al_2Au dendrites (Fig. 7). These are surrounded by an Al halo which becomes dendritic at higher rates. No haloes were observed in the hypoeutectic structures (Figs. 2 and 5). Eutectic structures (free-dendrites and interdendritic) are characterized by the presence of a colony structure at high velocities ($R > 4.7 \times 10^{-3}$ cm sec^{-1}). The segregation phenomena are important only in the case of

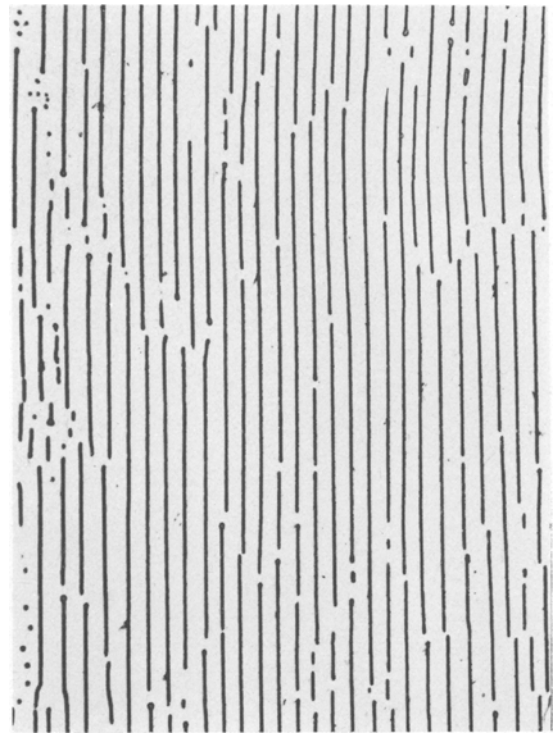

Figure 4 Broken lamellar structure (optical micrograph) in transverse section of Al–4.40 wt % Au specimen unidirectionally solidified at 1.6×10^{-4} cm sec^{-1} (× 200).

strongly hypereutectic alloys solidified at low velocities.

A point worth noting is that etching of polished surfaces, for morphological examination of the Al–Al_2Au alloys in the optical or scanning electron microscope, easily leads to the formation of Au precipitates as a consequence of the dissolution (by chemical reagents) of the Al_2Au intermetallic. Such a phenomenon, already observed elsewhere in the system Al–Au [21], is shown in Fig. 8 where Au is precipitated as fine colloidal particles retracing apparently the morphology of the original material.

3.2. Interphase spacing

The data of the interlamellar spacing are reported in the double-logarithmic plot (Fig. 9). The solid line is the best fit to experimental points obtained by the measurements carried out on free dendrite eutectic structures, while the dotted line are those points determined for interdendrite structures. The classical relationship $\lambda = A \cdot R^{-n}$ [22, 23], where A is a constant and n is an exponent having the theoretical value of 0.5, is verified with better approximation in the case of interdendritic eutectic ($n = 0.49$) than in the case of fully eutectic ($n = 0.37$).

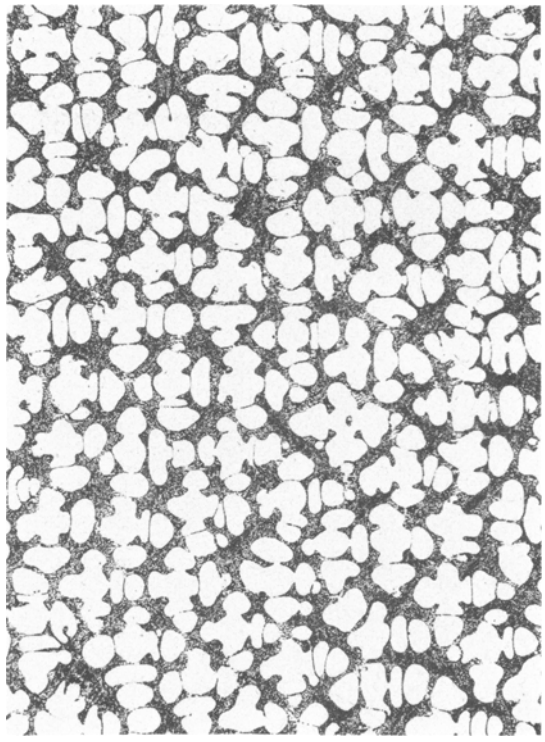

Figure 5 Hypoeutectic structure (optical micrograph) in transverse section of Al–4.71 wt % Au specimen unidirectionally solidified at 4.3×10^{-3} cm sec^{-1} (× 100).

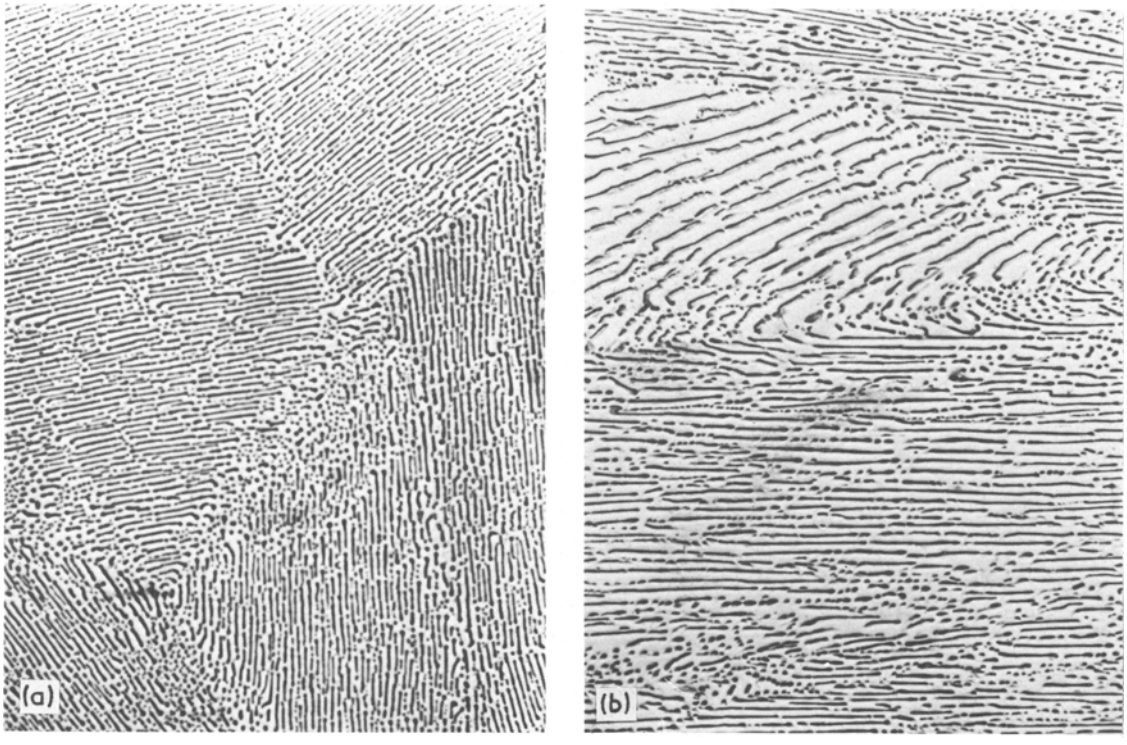

Figure 6 Eutectic structure (optical micrograph) on transverse (a) and longitudinal section (b) of Al–7.15 wt % Au specimen unidirectionally solidified at 2.55×10^{-3} cm sec^{-1} (× 200).

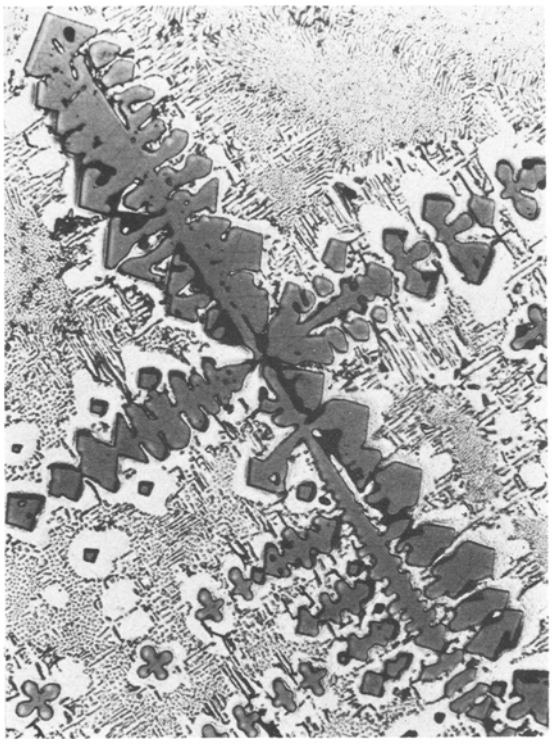

Figure 7 Faceted Al_2Au dendrites (optical micrograph) in transverse section of Al–15.35 wt % Au specimen unidirectionally solidified at 2.1×10^{-4} cm sec^{-1} (× 200).

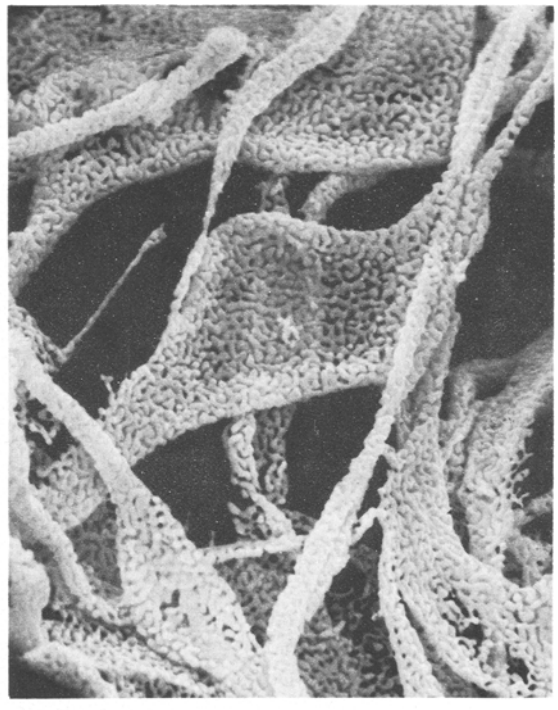

Figure 8 SEM image of residue after strong etching of transverse section of Al–6.68 wt % Au specimen unidirectionally solidified at 5.50×10^{-3} cm sec^{-1} (× 5000).

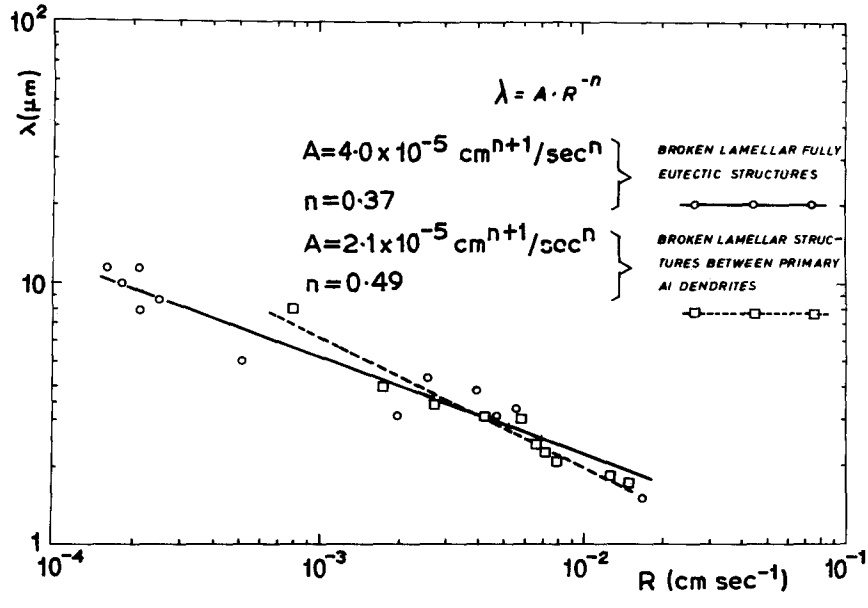

Figure 9 Logarithmic plot of the average value of interlamellar spacing (λ) as a function of solidification rate (R).

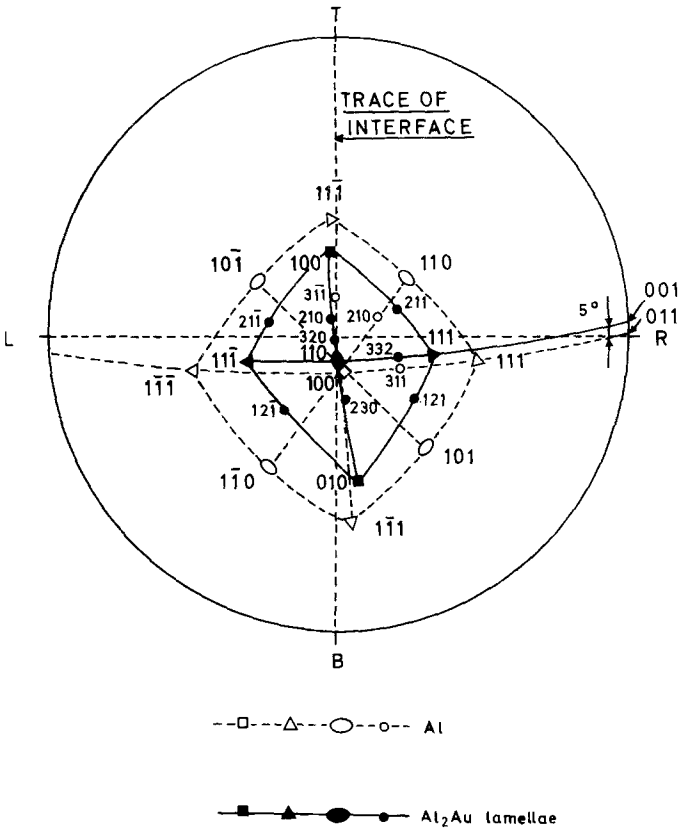

Figure 10 Crystallographic orientation data in lamellar Al–Al_2Au eutectic (plane of projection perendicular to growth direction).

3.3. Crystallography

The alloy phases have been identified using a 57.3 mm Guinier powder camera and monochromatised Cu$K\alpha$ radiations. The unit cell parameters, as obtained for Al and intermetallic phase Al_2Au, are 4.05 and 5.99 Å, respectively. The parameter of the Al-cell containing a small amount of Au-solute is found to be slightly greater than that of pure Al (4.04 Å), while the parameter of Al_2Au is identical to that of an Al_2Au sample prepared by solid diffusion of Al into Au at 300° C (ASTM Card 17-877). In no cases have additional reflections been observed which could be attributed to the presence of other components.

The crystallographic orientations were carried out in a Hilger Microfocus Unit using the back-reflection Laue method and a specimen-to-film distance of 30 mm. In this way the angular range of 2θ between 115 and 150° C could be successfully explored in relation to d-spacings varying from 0.90 to 0.80 Å. The Al spots could be distinguished from those of the Al_2Au phase by taking a number of photographs with filtered Cu$K\alpha$ radiation and with powdered Pt as internal standard. The orientation data, as obtained on different grains of eutectic lamellae as shown in Fig. 6a, are illustrated in Fig. 10.

The $[1\,0\,0]_{Al}$ and $[1\,1\,0]_{Al_2Au}$ directions are located near the centre of the stereogram. Since the plane perpendicular to the growth direction has been chosen as the plane of projection, these directions represent the growth directions of the two phases. The maximum angular deviation of $[1\,0\,0]_{Al}$ and $[1\,1\,0]_{Al_2Au}$ from the growth direction as observed on different grains is 11°. Moreover, the Al_2Au–$(0\,0\,1)$ pole and the Al–$(0\,1\,1)$ pole coincide with the interface-plane normal, within ~ 5°. The $(0\,0\,1)$–Al_2Au plane and the $(0\,1\,1)$–Al plane are the low-index planes closest to the interface, so that they may be considered as the contact planes. The atomic matching at the interface, as derived from the orientation data of the stereogram, is illustrated in Fig. 11. The above data may be summarized as follows:

lamellar interface

$$\|(0\,0\,1)_{Al_2Au}\|(0\,1\,1)_{Al}$$

$$[1\,1\,0]_{Al_2Au}\|[1\,0\,0]_{Al}$$

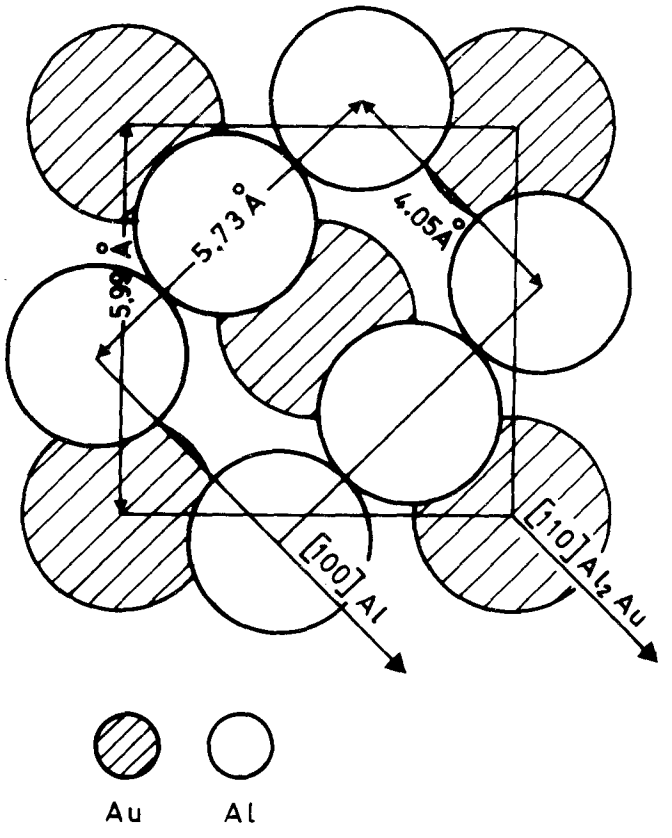

Figure 11 Schematic drawing of the atom matching at the lamellar interface of Al–Al_2Au eutectic.

growth direction $\parallel [1\,1\,0]_{Al_2\,Au} \parallel [1\,0\,0]_{Al}$.

A typical orientation stereogram as obtained from grains with a rod-type morphology (Fig. 3) is shown in Fig. 12. As far as the growth direction is concerned the conditions are similar to those observed in lamellar eutectics:

growth direction $\parallel \langle 1\,1\,0\rangle_{Al_2\,Au} \parallel \langle 1\,0\,0\rangle_{Al\ matrix}$.

In all cases examined here the [1 0 0] direction of the Al matrix was almost perfectly parallel to the growth direction, while the [1 1 0] direction of the Al_2Au rods deviated from the growth direction within an angular limit of 14°.

Laue back-reflection photographs taken on Al and Al_2Au dendrites like those shown respectively in Figs. 2 and 7 yield:

Growth direction $\parallel \langle 1\,0\,0\rangle_{Al\ dendrites}$

$\parallel \langle 1\,0\,0\rangle_{Al_2Au\ dendrites}$.

The results confirm earlier findings that dendrites of fcc metals grow preferentially along one of the [1 0 0] directions.

4. Discussion

The coupled growth zone skewed towards the Al_2Au side in the eutectic Al–Al_2Au (Fig. 1) is in agreement with the hypothesis of Hunt and Jackson [8] regarding the position of the coupled zone in a faceted/non-faceted system. The widening of the coupled zone at high G/R ratios corresponds to the region discovered by Mollard and Flemings [10], who suggested, for the eutectic range, the relation:

$$\Delta C = C_\infty - C_E = GD/mR \qquad (1)$$

where C_∞ is the alloy composition, C_E is the eutectic composition, D is the diffusion coefficient, m is the liquidus slope of one phase and G and R have the usual meanings. Taking $C_E = 5$ wt % Au, $m_{Al} \simeq 8.8°$ C/wt %, $m_{Al_2Au} \simeq 5.8°$ C/wt % from the Al–Au equilibrium diagram proposed by Hansen and Anderko [19] on the basis of a work of Ageew and Ageewa [24] and using a diffusion coefficient of $D = 6.7 \times 10^{-5}$ cm sec^{-1} [25] for all calculations, we obtained the calculated limits of the coupled region which are shown in Fig. 13 (curves B). Owing to the uncertainty of the exact location of the eutectic (Al corner) on the Al–Au

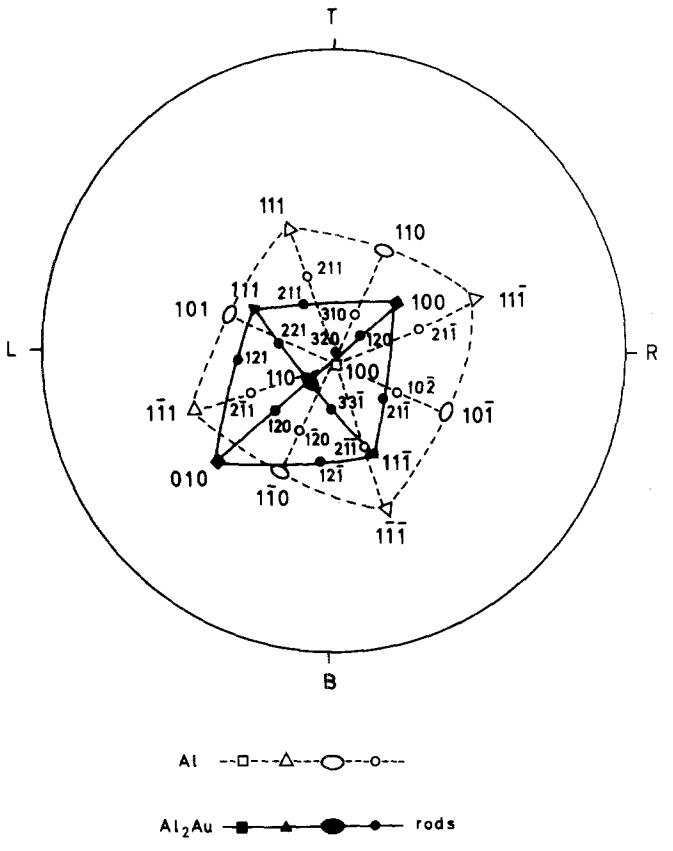

Figure 12 Crystallographic orientation of Al_2Au rods in Al–Al_2Au eutectic (plane of projection perpendicular to growth direction).

system, other curves (C) have been plotted in Fig. 13 using Equation 1, assuming $C_E = 7.5$ wt% Au, m_{Al} 5.9° C/wt% Au, m_{Al_2Au} 11.3° C/wt% Au, from an equilibrium diagram proposed by Hansen [26] on the basis of the work of Heycock and Neville [27]. From the comparison of experimental limits (A) with calculations (B) and (C) it is evident that for the boundaries between dendritic Al front and plane front there is poor agreement with curves B but good agreement with curves C, obtained from location at the eutectic point at 7.5 wt%. It appears then that the Mollard and Flemings model explains the experimental results quantitatively for the Al-rich side coupled growth boundaries and the eutectic compositions would be close to 7.5 wt%. For the Al_2Au-rich side, however, there is poor agreement between experimental curves (A) and theoretical curves (B) and (C). In this case, it would be useful to employ the more sophisticated model of Burden and Hunt [14]. In their competitive growth theory the eutectic range is given by

$$\Delta C = (1/m)\{(GD/R) + (B - A)R^{1/2}\} \quad (2)$$

where B and A are constants related to different parameters. In this relation the term $(B - A)R^{1/2}$ predominates at high velocities, and the couple growth is then proportional to $R^{1/2}$ and practically insensitive to G. In our case, $(B - A)R^{1/2}$ would thus modify curves C at low G/R ratios; unfortunately the short-comings of the various data do not permit the calculation of constant A (defined in [23]) of this term. It would also include the kinetics factors. These are generally omitted in faceted/non-faceted systems in order to obtain theoretically asymmetric coupled growth limits as shown by Fischer and Kurz in the Al–Si system [17].

Kerr and Winegard [28] pointed out that a broken lamellar morphology is typical of faceted/non-faceted systems in which the volume fraction of the intermetallic phase is low. Such a morphology was, therefore, expected in the present system. We may note that a broken lamellar eutectic is in contradiction to the Jackson and Hunt theory [23] which predicts a completely regular structure in faceted/non-faceted systems. However Fidler *et al.* [29] have recently reported

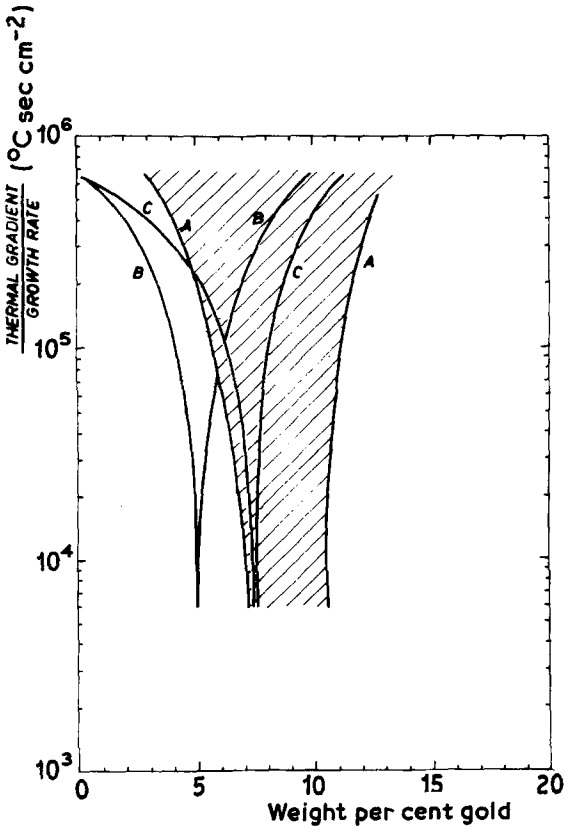

Figure 13 Comparison of experimental boundaries between dendritic and plane front structures (curves A from Fig. 1) and calculated boundaries (curves B and C from Equation 1). The curves B are drawn assuming eutectic composition C_E = 5.0 wt% [19, 24] and curves C are drawn taking C_E = 7.5 wt% [26, 27].

that the structure is completely regular in those eutectics where the phasic volume ratio is below 10:1, while the structure becomes broken-lamellar when this ratio exceeds this value. This is actually the case in the Al–Al_2Au system (phasic ratio $\simeq 50:1$).

The fact that a rod-type structure has also been obtained seems to be due to the influence of factors other than composition. A flake/fibre transition depending on growth rate and thermal gradient and not on composition, has been shown in Al–Si faceted/non-faceted systems by Day and Hellawell [30] and Steen and Hellawell [31]. In our case, the broken lamellar/rod transition seems also to be dependent on growth rate and not on composition, although in our case data at different thermal gradients are insufficient. This characterization of the flake/fibre transition proposed [30, 31] could be valid in the sense that it is related to growth anisotropy of the faceted phase.

4.2. Interphase spacings

The variation of average interlamellar spacing with growth rate (Fig. 9) corresponds to the classical relation $\lambda = AR^{-n}$ [22, 23], verified by several authors. The difference between the values of n corresponding respectively to the interdendrite eutectic and the free-dendrite eutectic is probably due to higher percentages of solute in the later morphologies.

4.3. Crystallography

Any attempt to discuss the crystallographic orientation data in terms of interfacial energies is rather difficult because the factors determining the energy of a particular interphase are imperfectly understood at present. It is generally assumed that lamellar growth is favoured if the phases grow in such a way as to select interfaces of lowest possible energy. According to Kraft [32, 33], a low energy interface is parallel to crystallographic planes of wide spacing and nearly equal atomic densities in the two phases. The repeat distance on the $(0\,0\,1)_{Al_2Au}$ plane is 2.99 Å. This is comparable with 2.88 Å which is the repeat distance on the $(0\,1\,1)_{Al}$ plane along the [0 1 1] direction. The densities of atoms lying exactly on the $(0\,0\,1)_{Al_2Au}$ plane and on the $(0\,1\,1)_{Al}$ plane, are 0.14 and 0.25 atom $Å^{-2}$ respectively. The schematic drawing of the atomic matching at the lamellar

interface (Fig. 11) supposes that the strain present at the interface due to the mismatching of the two lattices is relatively low, so that the conditions for a low energy interface may be present in the lamellar eutectics. Unfortunately, the interfacial relationship could not be successfully determined in the case of the grains with a rod-type morphology, because of the facets on the rods were not sufficiently well developed to give a reliable interface trace. One may note from Fig. 12, however, that the mutual orientation of the Al_2Au and Al-cells is such that no low-index crystallographic planes are strictly parallel to each other. Such as orientation implies a relatively high-energy interphase, with respect to that of the lamellar eutectic considered before. Therefore, it would not be surprising if the rod-type structure is remarkably less stable than the lamellar structure.

5. Conclusions

(1) In the considered composition range between 4.10 and 15.35 wt % Au and for growth rates varying from 1.6×10^{-4} to 1.66×10^{-2} the Al–Al_2Au unidirectionally solidified eutectic is characterized by a broken lamellar type structure which at lower solidification rates contains grains of ordered or randomly distributed faceted rods.

(2) Al–Al_2Au system exhibits a coupled growth zone skewed toward the Al_2Au-rich side (hypereutectic compositions). The widening of the zone at lower solidification rates and high thermal gradients corresponds to the region discovered by Mollard and Flemings.

(3) The well known relationship $\lambda = A \cdot R^{-n}$ between interlamellar distances and solidification rates has been found to be valid over the whole range of compositions considered, ($n = 0.37$ for free-dendrite eutectic and $n = 0.49$ for the interdendrite eutectic).

(4) The preferred crystallographic direction of growth of the Al_2Au lamellae and the Al_2Au rods is the [1 1 0] direction. Dendrites of Al and of the intermetallic Al_2Au grow preferentially along the ⟨1 0 0⟩ direction.

(5) The interface relationships of eutectic alloys with lamellar morphology are

lamellar interface $\quad \| (0\,0\,1)_{Al_2Au} \| (0\,1\,1)_{Al}$

$\quad [1\,1\,0]_{Al_2Au} \| [1\,0\,0]_{Al}$

Growth direction $\quad \| [1\,1\,0]_{Al_2Au} \| [1\,0\,0]_{Al}$.

(6) The crystallographic orientation data suggest that the conditions for a low energy interface are approached in the case of lamellar eutectics, while low energy equilibrium conditions do not seem to be reached in the case of rod-type morphologies.

Acknowledgements

The authors are indebted to Professor Kurz (Ecole Polytechnique Fédérale, Lausanne) for his helpful criticism and advice. Thanks are also due to Soc. Siemens, Milano for the operation of the scanning electron microscope. Technical assistance was rendered by Dr G. Serrini (Chemical analysis), Mr D. Boerman (calculations), Mr E. Haine (metallography) and Mr A Misirocchi (unidirectional solidification).

References

1. G. A. CHADWICK Spec. Publ. 110 (Iron & Steel Inst., London, 1968) p. 138.
2. A. HELLAWELL, *ibid*, p. 155.
3. L. M. HOGAN, R. W. KRAFT and F. D. LEMKEY, "Advances in materials Research" Vol. 5 (Wiley, New York, 1971) p. 83.
4. J. D. LIVINGSTON, *Mater. Sci. Eng.* 7, (1971) 61.
5. W. KURZ and P.R. SAHN, "Gerichtet erstarrte euteckische Werkstoffe" (Springer, Berlin, 1975).
6. G. TAMMANN and A. A. BOTSCHWAR, *Z. Anorg. Chem.* **157** (1926) 26.
7. A. KOFLER, *Z. Metallk.* **41** (1950) 221.
8. J. D. HUNT and K. A. JACKSON, *Trans. Met. Soc. AIME* **239** (1967) 864.
9. H. E. CLINE and J. D. LIVINGSTON, *ibid* **245** (1969) 1987.
10. F. R. MOLLARD and M. C. FLEMINGS, *ibid* **239** (1967) 1526.
11. R. M. JORDAN and J. D. HUNT, *Met. Trans.* 2 (1971) 3401.
12. H. E. CLINE, *Trans. Met. Soc. AIME* **242** (1968) 1613.
13. D. T. J. HURLE and E. JAKERMAN, *J. Crystal Growth* **3**, 4 (1968) 574.
14. M. H. BURDEN and J. D. HUNT, *ibid* **22** (1974) 328.
15. K. A. JACKSON, *Trans. Met. Soc. AIME* **242** (1968) 1275.
16. H. A. H. STEEN and A. HELLAWELL, *Acta Met.* **23** (1975) 529.
17. D. J. FISHER and W. KURZ, Communication at "Sixth International Light Metals Conference" Leoben – Vienna, Austria, June 1975.
18. G. BEGHI and G. PIATTI, Communication at "XIV Convegno Nazionale A.I.M.", Trieste, Italy (1970).
19. M. HANSEN and K. ANDERKO, "Constitution of Binary Alloys" (McGraw-Hill, New York, 1958) p.75.
20. K. N. STREET, C.F. ST. JOHN and G. PIATTI, *J. Inst. Metals* **95** (1967) 326.
21. M. VON HEIMENDAHL, *Praktische Metallographie* **4** (1967) 65.

22. W. A. TILLER, "Liquid Metals and Solidification" (ASM, Cleveland, Ohio, 1958).
23. K. A. JACKSON and J. D. HUNT, *Trans. Met. Soc. AIME* **236** (1966) 1129.
24. N. AGEEW and V. AGEEWA, *ibid* **128** (1938) 259.
25. J. FORSTEN and H. M. MIEKK-OJA, *J. Inst. Metals* **99** (1971) 105.
26. M. HANSEN, "Der Aufbau der Zweistofflegierungen" (Springer, Berlin, 1936).
27. C. T. HEYCOCK and F. H. NEVILLE, *Phil. Trans. Roy. Soc. A* **194** (1900) 201; **214A** (1914) 267; *Proc. Roy. Soc.* **90** (1914) 560.
28. H. W. KERR and W. C. WINEGARD, *Canad. Met. Q.* **6** (1967) 55.
29. R. J. FIDLER, M. N. CROKER and R. W. SMITH, "Crystal Growth" (North Holland, Amsterdam, 1971) p. 739.
30. M. G. DAY and A. HELLAWELL, *Proc. Roy. Soc. A* **305** (1968) 473.
31. H. A. H. STEEN and A. HELLAWELL, *Acta Met.* **20** (1972) 363.
32. R. W. KRAFT, *Trans. Met. Soc. AIME* **224** (1962) 65.
33. *Idem, ibid* **227** (1963) 393.

Received 5 March and accepted 6 October 1975.